The Journal of Immunology

# Anti-CD20 Antibody with Multimerized Fc Domains: A Novel Strategy To Deplete B Cells and Augment Treatment of Autoimmune Disease



Xiaoyu Zhang, Henrik S. Olsen, Shaodong Chen, Edward So, Hua Zhou, Erin Burch, Emmanuel Y. Mérigeon, David S. Block and Scott E. Strome

*J Immunol* 2016; 196:1165-1176; Prepublished online 22 December 2015;
doi: 10.4049/jimmunol.1501755
http://www.jimmunol.org/content/196/3/1165



*The Journal of Immunology* is published twice each month by
The American Association of Immunologists, Inc.,
1451 Rockville Pike, Suite 650, Rockville, MD 20852

Print ISSN: 0022-1767 Online ISSN: 1550-6606.

# Anti-CD20 Antibody with Multimerized Fc Domains: A Novel Strategy To Deplete B Cells and Augment Treatment of Autoimmune Disease

**Xiaoyu Zhang,* Henrik S. Olsen,† Shaodong Chen,‡ Edward So,* Hua Zhou,* Erin Burch,* Emmanuel Y. Mérigeon,† David S. Block,† and Scott E. Strome***

**We developed a fully recombinant anti-CD20 protein derived from cDNA encoding one Fab domain, two IgG1 Fc regions, the IgG2 hinge, and an isoleucine zipper. This protein, called GB4542, contained both the homodimer and higher-order multimers. Binding studies revealed that GB4542 preferentially bound $CD20^+$ cells yet also recognized $CD20^-Fc\gamma R^+$ PBMC. In contrast, a control mAb containing the identical Fab region, GB4500, failed to bind $CD20^-Fc\gamma R^+$ PBMC. Consistent with these findings, interactions between GB4542 and the canonical Fc$\gamma$Rs had substantially lower $K_D$ values than correlate interfaces between GB4500 and these receptors. At low concentrations, GB4542 showed enhanced Ab-dependent cellular cytotoxicity, Ab-dependent cellular phagocytosis, and complement-dependent cytotoxicity compared with GB4500. However, at higher concentrations, an Fc analog of GB4542 inhibited anti-CD20 mAb–mediated B cell clearance through direct blocking of both Fc–Fc$\gamma$R interactions and C1q deposition on target cells. Furthermore, the higher-order multimer fraction of GB4542 demonstrated greater binding avidity with the canonical Fc$\gamma$Rs and was associated with inhibitory effects observed in Ab-dependent cellular phagocytosis and complement-dependent cytotoxicity assays. These data suggest that GB4542 might have utility in the treatment of autoimmune diseases by combining both mAb-mediated B cell depletion and multimerized Fc-mediated tolerogenic effects.** ***The Journal of Immunology*****, 2016, 196: 1165–1176.**

The chimeric anti-CD20 Ab, rituximab, together with methotrexate, is approved for the treatment of rheumatoid arthritis that is refractory to TNF blockade. Despite the therapeutic efficacy of rituximab and methotrexate combinations, the majority of responding patients evidence only a 20% improvement in disease severity (American College of Rheumatology 20) (1–4). Because rituximab results in near-complete and long-lasting B cell depletion, both in the periphery and in secondary lymphoid organs (5, 6), efforts to improve outcomes by increasing potency are likely to meet with limited success (4). Furthermore, the discordance between the ability of rituximab to mediate rapid B cell depletion in vivo (7, 8) (hours to days) and the delay in maximal treatment effect (weeks to months) implies that downstream effects of B cell loss likely contribute to clinical improvement (9). Based on these observations, recent studies have tested the hypothesis that the use of rituximab in combination with other immunomodulatory agents may provide additive or synergistic therapeutic benefit (10).

One drug which, in combination with rituximab, has shown preliminary utility for the treatment of select autoimmune diseases and allograft rejection is pooled human IVIG. The combination of IVIG and rituximab has evidenced striking therapeutic value in refractory pemphigus vulgaris (11) and recalcitrant ocular cicatricial pemphigoid (12). Similarly, treatment of Ab-mediated graft rejection with plasmapheresis in combination with IVIG and rituximab is more effective than IVIG alone (13–15). Unfortunately, implementation of phase III trials to evaluate the efficacy of the combination of IVIG and rituximab versus either agent alone are hindered by the limited availability of IVIG and the high cost of these drugs.

One potential means to overcome some of the practical challenges of IVIG/rituximab therapy would be to develop a reagent capable of combining the anti-inflammatory properties of both drugs. Development of such a drug has been hindered by debate surrounding the mechanism(s) by which IVIG mediates its anti-inflammatory effects. However, several reports suggest that many of the tolerogenic properties of IVIG can be recapitulated by Fc aggregates (16–24). As a first step in translating the use of Fc aggregates into clinical practice, we created fully recombinant murine Fc multimers, termed stradomers, which are composed of the Fc fragment of mouse IgG2a and a human IgG2 multimerization domain, and demonstrated that these compounds can effectively treat idiopathic thrombocytopenic purpura and collagen-induced arthritis in mice (25). The anti-inflammatory properties of these or similar stradomers have been reproduced by other investigators in murine models of experimental autoimmune neuritis and myasthenia gravis (26, 27).

*Department of Otorhinolaryngology–Head and Neck Surgery, University of Maryland School of Medicine, Baltimore, MD, 21201; †Gliknik Inc., Baltimore MD, 21201; and ‡Medical College of Xiamen University, Xiamen 361005, China

ORCID: 0000-0003-4727-5135 (S.C.).

Received for publication August 5, 2015. Accepted for publication November 16, 2015.

This work was supported by Gliknik through a sponsored Research Agreement with the University of Maryland Baltimore and National Cancer Institute Contract HHSN261201100103C. S.C. was supported by the Medical College of Xiamen University.

Address correspondence and reprint requests to Dr. Scott E. Strome, Department of Otorhinolaryngology–Head and Neck Surgery, University of Maryland School of Medicine, 16 South Eutaw Street, Suite 500, Baltimore, MD, 21201. E-mail address: sstrome@smail.umaryland.edu

The online version of this article contains supplemental material.

Abbreviations used in this article: 7-AAD, 7-aminoactinomycin D; ADCC, Ab-dependent cellular cytotoxicity; ADCP, Ab-dependent cellular phagocytosis; CDC, complement-dependent cytotoxicity; CHO, Chinese hamster ovary; DI, deionized; EGFR, epidermal growth factor receptor; IC, immune complex; ILZ, isoleucine zipper; sAb, stradobody; SF, stable fraction; SPR, surface plasmon resonance; TF, transient fraction.

Based on the ability of these multimerized Fc compounds to avidly bind the low-affinity FcγRs on effector cells (e.g., NK cells, monocytes, and macrophages), we initially hypothesized that linkage to a Fab fragment directed against a tumor Ag (e.g., the epidermal growth factor receptor [EGFR]) would result in more potent antitumor immunity. Indeed, our studies revealed that anti-EGFR stradobodies (sAb), characterized by an anti-EGFR Fab linked to a multimerized Fc domain, mediated enhanced complement-dependent cytotoxicity (CDC) and Ab-dependent cellular cytotoxicity (ADCC) of EGFR-expressing colon cancer cell lines in vitro (28). However, we postulated that, like the stradomers, in the absence of Ag, the ability of the multimerized Fc fragments of the stradobodies to engage FcγRs and complement might prove tolerogenic.

In order to test this hypothesis, we employed a fully recombinant human anti-CD20 sAb, termed GB4542. GB4542 effectively competed with rituximab for CD20 binding and engaged both FcγRs and C1q, independent of Fab–Ag interactions. At low concentrations, GB4542 was more potent than a conventional anti-CD20 mAb control, GB4500, in mediating B cell depletion by CDC, ADCC, and macrophage phagocytosis (Ab-dependent cellular phagocytosis [ADCP]). Consistent with our hypothesis, at higher concentrations, an sAb with an Fc fragment identical to GB4542, but for which Fab fragment targeted an irrelevant Ag, inhibited rituximab-mediated B cell killing. The mechanisms by which GB4542 inhibited ADCC, ADCP, and CDC were both overlapping with and distinct from IVIG. Our data suggest that GB4542 may serve as an effective means to mediate B cell depletion and induce secondary tolerance.

## Materials and Methods

### *Cells and reagents*

Buffy coats from healthy donors were purchased (Biological Specialty Corporation, Colmar, PA), and PBMC were prepared by density centrifugation (Ficoll-Paque; Amersham). Monocytes, B lymphocytes, and NK cells were purified from PBMC by negative selection using the monocyte isolation kit II, B cell isolation kit II, and NK cell isolation kit (Miltenyi Biotec, Auburn, CA) according to the manufacturer's instructions. B cell depletion was performed using CD19 microbeads (Miltenyi Biotec). The purity of cell separations was typically >95% for monocytes and B lymphocytes, >90% for NK cells, and >80% for B cell depletion as assessed by flow cytometry. In vitro cell cultures were performed in RPMI 1640 (CellGro) supplemented with 2–10% FCS (Atlantic Biologicals, Miami, FL), 1% penicillin/streptomycin, 1% HEPES, and 1% Glutamax (all from Life Technologies). IVIG was purchased from Atlantic Biologicals. Human complement was purchased from Cedarlane Laboratories (Burlington, NC).

### *Generation and production of the mAb and sAb*

The anti-CD20 mAb and GB4542 sAb constructs were generated essentially as described (28). The amino acid sequence for rituximab was obtained from the ImMunoGeneTics database (http://www.imgt.org), and DNA fragments were synthesized at Blue Heron Biotechnology (Bothell, WA). G001, recombinant human IgG1 Fc; GL-2045, recombinant human IgG1 multimer; GB2500, recombinant anti–Her-2 mAb; and GB2542, recombinant anti–Her-2 sAb were all prepared by Gliknik (Baltimore, MD) (25, 28).

### *Preparation of sAb fractions by gel filtration*

GB4542 Chinese hamster ovary (CHO) transient and GB4542 CHO stable pool supernatants were purified by affinity chromatography with protein A HiTrap MabSelect Sure (#11-0034-95; GE Healthcare) followed by a first wash with binding buffer (20 mmol sodium phosphate and 0.15 mol NaCl [pH 7.2]) and a second wash with 1 mol NaCl, 5 mmol EDTA, 2 mol urea, and 50 mmol phosphate (pH 7). The elution step was performed with 0.1 mol glycine (pH 2.7). Eluate was desalted in 1× PBS and 200 mmol NaCl (pH 7.4) using a HiPrep 26/10 column (#17-5087-01; GE Healthcare). After concentration and buffer exchange with running buffer (0.05 mol Tris-HCl + 0.15 mol NaCl [pH 7.5]), GB4542 (≤5 ml) was loaded onto the gel filtration column (Hiload 26/60 Superdex 200 pg; #17-1071-01; GE Healthcare) and separated in running buffer. Fractions from transient (TF) and stable (SF) pools were then identified by SDS-PAGE and dialyzed against 1× PBS 150 mmol NaCl (pH 7).

### *SDS-PAGE analysis*

*Nondenatured samples.* A total of 2 μg protein diluted in 3 μl sample buffer (NuPage; LDS [4×], #NP0007; Life Technologies), 20 μmol iodoacetamide (#163-2109; Bio-Rad), and deionized (DI) water (to obtain 10 μl as final volume) were heated at 80°C for 10 min. A total of 10 μl HiMark Pre-Stained Protein Standard (#LC5699; Life Technologies) was used as m.w. marker. Samples were loaded onto the gel (NuPage 3–8% Tris-Acetate, #EA03752BOX; Life Technologies) and run at 150 V for 1 h and 25 min using Tris-acetate SDS running buffer (#LA0041; Life Technologies).

*Denatured samples.* A total of 0.75 μg protein diluted in 3 μl sample buffer (NuPage, LDS [4×], #NP0007; Life Technologies), 2 μl reducing agent (NuPage #NP004; Life Technologies), and DI water (to obtain 10 μl as final volume) was heated at 70°C for 10 min. A total of 10 μl Novex Sharp Pre-Stained Protein Standard (#LC5800; Life Technologies) was used as m.w. marker. Samples were loaded onto gel (NuPage 12% Bis-Tris, #NP0342BOX; Life Technologies) and run at 150 V for 2 h using MOPS SDS running buffer (#NO0001-02; Life Technologies). Gels were washed in DI water, stained with SimplyBlue Safe (#LC6060; Life Technologies), and destained in DI water.

### *Surface plasmon resonance*

Surface plasmon resonance (SPR) experiments were performed in a Biacore 3000 instrument (GE Healthcare). Mouse anti-histidine (GE Healthcare) was immobilized to all four flow cells on a CM5 chip to 6000 RU per the manufacturer's instructions. Using HBS-EP as running buffer, C-terminally histidine-tagged FcγRI and FcγRIIIa (158F) or FcγRIIb and FcγRIIa (R&D Systems) were captured on flow cells 2 and 4, respectively. For FcγRI and FcγRIIIa, GB4542 and GB4500 were serially diluted from 6.25 to 0.0004 nmol and 200 to 0.0128 nmol, respectively. For FcγRIIa and FcγRIIb, GB4542 and GB4500 were serially diluted from 625 to 0.2 nmol and from 5000 to 0.32 nmol, respectively. Both GB4542 and GB4500 were injected at increasing concentrations at 25 μl/min for 3 min over all flow cells, followed by a 5-min dissociation phase. After each injection, all flow cells were regenerated with 10 mmol glycine (pH 1.5) for 1 min at 50 μl/min followed by a 1-min wash. Flow cells 1 and 3 served as reference subtraction surfaces. Blank runs were subtracted from each curve. Kinetics were calculated using the 1:1 Langmuir Binding logarithm with refractory index set to 0 in the BIAevaluation software v.3.1. All curves were run in triplicate.

SPR analysis of GB4542 fractions were performed on a separate chip using the same methods as above. For FcγRI and FcγRIIIa, GB4542 fraction 2 and 4 were serially diluted from 1.5 to 0.023 nmol. For FcγRIIa and FcγRIIb, GB4542 fraction 2 was serially diluted from 750 to 5.9 nmol, and GB4542 fraction 4 was serially diluted from 150 to 0.29 nmol.

The molar concentrations of GB4500, GB4542, GB4542 fraction 2, and GB4542 fraction 4 were based on estimated molecular weights of 150, 400, 400, and 600 kDa, respectively. Importantly, because each of these preparations contained more than one component, the $K_D$s are estimates.

### *Flow cytometry*

Fluorochrome-labeled mAbs anti-human CD3, CD19, and CD11b were obtained from BioLegend; anti-human CD56, CD14, CD16, CD32, and isotype controls were obtained from BD Biosciences; and anti-human C1q mAb was purchased from Cedarlane Laboratories. Dylight 488–labeled G001, GL-2045, GB4500, GB4542, GB2500, and GB2542 were prepared in-house using the Dylight 488 microscale Ab labeling kit (Thermo Scientific) per the manufacturer's protocol. Labeled cells were acquired on an LSRII flow cytometer (BD Biosciences) and analyzed with FACS Diva (BD Biosciences) and FlowJo software (Tree Star). For analysis, the lymphocyte, monocyte, and granulocyte populations were first gated based on forward and side scatter. Human peripheral blood B cells were defined as $CD3^-CD19^+$, NK cells as $CD3^-CD56^+$, monocytes as $CD14^+$, and granulocytes as $CD16^+$.

### *FcγR-expressing CHO cell lines and CHO cell binding assays*

OmicsLink Expression Clones encoding human FcγRIIa, FcγRIIb, and FcγRIIIa were purchased from GeneCopoeia (Rockville, MD), transfected into CHO cells by Lipofectamine 3000 (Invitrogen), and cultured in selection media. FcγRIIa, FcγRIIb, and FcγRIIIa-expressing CHO cell clones were obtained by limiting dilution, and surface expression of FcγR

genes was verified by FACS staining using anti-CD32 (FcγRIIa, and FcγRIIb) and anti-CD16 (FcγRIII) mAb.

To compare the binding of GB4500 and GB4542 with FcγRs, CHO cells expressing individual FcγRs were incubated with Dylight 488–conjugated GB4500 or GB4542 at various concentrations for 30 min at 4°C. Cells were then washed and analyzed by flow cytometry.

### *Inhibition of GL-2045 binding to FcγR-expressing CHO cells*

CHO cells expressing human FcγRs were incubated with serial dilutions of GB4500/GB4542/IVIG for 15 min at room temperature, followed with a second-step incubation with Dylight 488–labeled GL-2045 (10 μg/ml) for 30 min at 4°C. The binding of GL-2045 with FcγRs on expressing CHOs was assessed by FACS analysis.

### *Colocalization studies*

Monocytes were cultured with 50 ng/ml M-CSF for 7 d. The resulting macrophages were harvested and reseeded at $2 \times 10^4$/chamber of an eight-chamber slide. After 24 h, cells were incubated for 60 min in the presence of 10 μg/ml or 0.1 μg/ml Dylight 488–conjugated GB4542 or GB4500 and PE-conjugated CD32 (clone FUN-2; BioLegend). At the end of the incubation, cells were fixed with 4% paraformaldehyde PBS for 30 min, then washed three times in PBS, permeabilized, and blocked with PBS + 0.1% saponin + 1% BSA for 1 h at room temperature. Cells were then incubated for 15 min with DAPI, washed, mounted with anti-fade, and stored at 4°C. Images were acquired on an Olympus FluoView 500 confocal microscope (Olympus) fitted with standard excitation and emission filters using a 40× objective.

### *C1q ELISA and C1q cell-surface deposition*

A 96-well plate (Immulon) was coated with C1q (Sigma-Aldrich) at 1 μg/ml overnight in PBS. After coating, the plate was washed three times with standard wash buffer (PBS + 0.05% Tween 20) and blocked with blocking buffer (1% BSA–0.05% PBS Tween) for 2 h at room temperature. Following blocking, the plate was incubated with stradobodies diluted in 100 μl/well blocking buffer and washed three times with standard washing buffer. The C1q-bound compound was detected by incubation with 1:5000 biotinylated mouse α-human IgG1 (BD Biosciences) and 100 μl/well Streptavidin-HRP (Southern Biotechnology Associates) for 1 h at room temperature. The plate was subsequently washed three times with washing buffer, after which color was developed with the TMB method (BD Biosciences) according to the manufacturer's protocol. Absorbance was read at 450 nm.

To measure C1q deposition, B cells were treated with Ab or sAb for 15 min in the presence of 10% human complement. Complement activation was terminated by addition of EDTA at 10 mmol, and cells were harvested and stained with FITC-conjugated anti-human C1q mAb and analyzed by flow cytometry.

### *Cytokine ELISA*

Cell-culture supernatants were collected 48 h after stimulation. LPS (Sigma-Aldrich) was added at 10 ng/ml for the last 24 h. The concentrations of IL-6 and -10 (BioLegend) and IL-12 and TNF-α (BD Biosciences) were measured by a standard ELISA, following the manufacturer's protocol.

### *Complement-dependent cytotoxicity*

Target cells ($2 \times 10^5$) were incubated in 96-well plates with various concentrations of mAb, sAb, or IVIG for 1 h at 37°C in the presence of human complement at a final concentration of 10% (v/v). To test the inhibition of CDC, B cells were pretreated with GB2542 or IVIG in the presence of human complement for 15 min, and GB4500 was then added directly to the culture at 1 μg/ml to induce CDC. Cytotoxicity was measured by FACS analysis of Annexin V/7-aminoactinomycin D (7-AAD) fluorescence (Annexin V–PE apoptosis detection kit I; BD Biosciences) according to the manufacturer's instructions.

### *Ab-dependent cytotoxicity*

In vitro cytotoxicity was evaluated using NK cells as effectors against autologous B cells as targets. Drugs tested included IVIG, GB4500, and GB4542. Target cells were incubated with 50 μCi chromium (Amersham, Piscataway, NJ) at 37°C for 1 h, mixing occasionally, and washed twice with complete media. Test Abs were added to 96-well plates with a final concentration ranging from 100 to 0.001 μg/ml serially diluted 10-fold, in duplicate, in a total volume of 200 μl for each well. Target and effector cells were added at a 20:1 E:T ratio. In the inhibition experiment, GB2542 or control Abs were added to the coculture of NK cells and B cells in the presence of 1 μg/ml GB4500. After incubation at 37°C in 5% $CO_2$ for 4 h, 100 μl cell lysis supernatant was collected and mixed with 100 μl Optiphase Supermix scintillation fluid (PerkinElmer, Boston, MA). Scintillation was measured in a MicroBeta 1450 scintillation counter (Vallac, Turku, Finland). Results are conveyed as the percentage of specific lysis according to the following formula:

$$\%\ \text{lysis} = [(\text{experimental cpm} - \text{spontaneous cpm}) \times 100]/(\text{maximum cpm} - \text{spontaneous cpm}).$$

### *Phagocytosis assays*

Purified peripheral blood monocytes were cultured in six-well plates at $1 \times 10^6$ cells/well in complete RPMI 1640 medium supplemented with 50 ng/ml M-CSF (BioLegend) for 6–8 d to induce macrophage differentiation. CFSE-labeled (Molecular Probes) B cells were cultured with macrophages at a 5:1 ratio in the presence of various concentrations of mAb, sAb, or IVIG in 96-well ultra-low attachment plates (Corning). In the sAb inhibition experiment, GB2542 or control Ab was added to the coculture of macrophages and B cells in the presence of 0.1 μg/ml GB4500. At the end of the 1-h incubation at 37°C, cells were harvested, stained with PE-conjugated anti-CD11b mAb for 30 min at 4°C, washed, and analyzed by FACS. Doublets were excluded using forward scatter height and width properties. The capacity of macrophages to phagocytose target cells was calculated as the percentage of CFSE/CD11b double-positive cells relative to the total macrophage population.

### *PBMC B cell depletion assay*

A total of $2 \times 10^5$ freshly isolated PBMCs were cultured with serial dilutions of mAb, sAb or IVIG at concentrations ranging from 0.001–100 μg/ml in a 96-well plate. After 48 h incubation at 37°C, cells were harvested and stained with cell-surface markers, followed by Annexin V/7-AAD, and analyzed for B cell apoptosis/death. Live B cells were defined as $CD3^-/CD19^+$/Annexin $V^-$/7-$AAD^-$ within lymphocyte gate. Accucount particles (Spherotech, Lake Forest, IL) were added before analyzing samples to obtain accurate absolute cell numbers. B cell depletion was calculated using the formula: % B cell depletion = (1 − live B cell number [treated]/[nontreated control]) × 100.

### *Statistical analysis*

Statistical analysis was performed by student *t* test. Differences were considered significant at a $p$ value $<0.05$.

## Results

### *GB4542 effectively engages CD20-positive B cells and competes with an anti-CD20 mAb for CD20 binding*

Each H-chain of GB4542 consists of the Fab sequence of rituximab and two IgG1 Fc domains separated by an isoleucine zipper (ILZ) and the IgG2 hinge (Fig. 1A) (28). Based on the knowledge that both the IgG1 H-chain and the Fc homodimer of IgG1 are ∼50 kDa, we expected that the molecular mass of the H-chain of GB4542 would be slightly >75 kDa (50 kDa [IgG1 H-chain] + 25 kDa [50% of IgG1 Fc homodimer] + 7 kDa [ILZ + IgG2H]). Consistent with these expectations, analysis of GB4542 by SDS-PAGE, under reducing conditions, revealed an H-chain band ∼80 kDa and an L-chain band at ∼25 kDa (Fig. 1B). The nonreduced gel revealed a weak band running between 171 and 238 kDa, a conglomerate of three intense bands running between 268 and 460 kDa, and a less intense band at ∼460 kDa.

In order to better delineate the species contained within GB4542, we fractionated the entire GB4542 preparation into predominantly low and high m.w. moieties by gel filtration, fractions 1–4 (Fig. 1B). The nonreduced gel revealed that these fractions had different migratory properties. Importantly, under reducing conditions, TF2, TF3, and TF4 demonstrated the same H-chain band as the nonfractioned protein at ∼80 kDa. These data suggested that the different fractions or bands of these proteins likely represent different levels of multimerization and that the proteins were covalently linked. Finally, a number of smaller m.w. moieties were present in TF1, which, based on their negligible presence in the

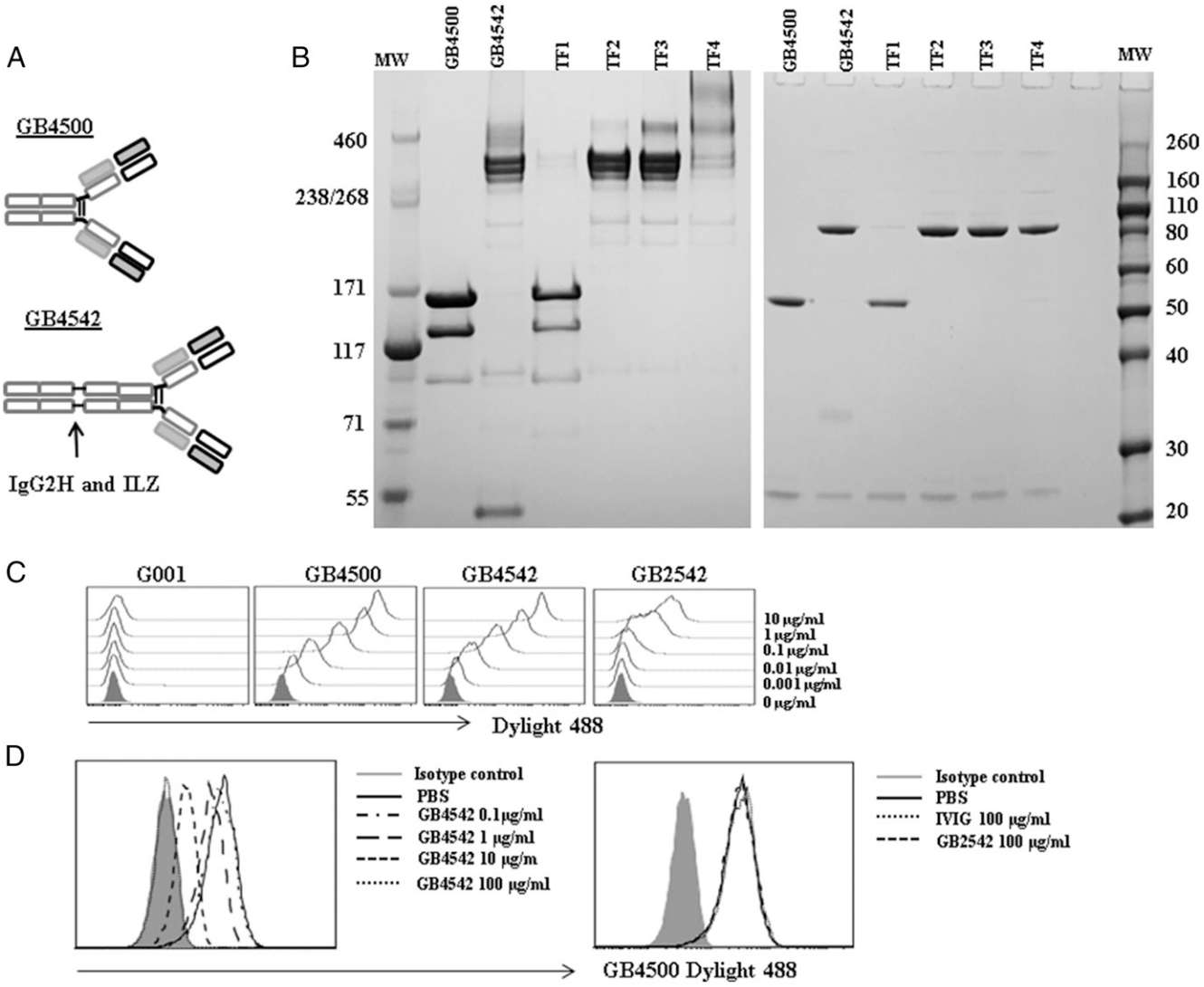


**FIGURE 1.** GB4542 effectively multimerizes and binds CD20$^+$ B cells. (**A**) GB4542 is a novel Fc-modified anti-CD20 mAb (sAb) incorporating an Fab identical to rituximab and an Fc region containing two human IgG1 Fc domains separated by the IgG2 hinge and the ILZ. (**B**) SDS-PAGE of GB4500, GB4542, and GB4542 fractions 1–4 (TF1–4) under nonreduced and reduced conditions. (**C**) Binding of GB4500, GB4542, and GB2542 to purified peripheral blood B cells. Purified PB B cells were incubated with serial dilutions of Dylight 488–conjugated mAb or sAb and analyzed by flow cytometry. Data are shown as histogram overlay of each Ab's binding with B cells at different concentrations. Filled histogram showed no staining control. (**D**) Blocking of GB4500 binding on Ramos cells by GB4542. Ramos cells were preincubated with GB4542 at serial dilutions from 0.1–100 μg/ml for 30 min at 4°C (*left panel*), followed by staining with Dylight 488–labeled GB4500 (1 μg/ml), and analyzed by flow cytometry. IVIG and GB2542 at 100 μg/ml were used as control (*right panel*). The data represent one of three experiments (C and D).

unfractionated preparation, were thought to represent alternatively assembled/processed proteins.

Next, to develop a higher-fidelity protein product, we created a stable GB4542-producing cell pool using technology from ExcellGene SA (Monthey, Switzerland), with all restriction sites removed, and fractionated the product. Nonreduced SDS-PAGE analysis showed four predominant bands, all of which were present in the transient material, but at different ratios (Supplemental Fig. 1). Specifically, distinct bands were present at the anticipated sizes for the homodimer and higher-order multimers. Furthermore, bands >460 kDa were present in fraction 4 derived from both the transient and stable pools. The smaller species present in fraction 1 of the transient material was not evident in the protein product from stable transfectants. Collectively, these data demonstrate that: 1) GB4542 formed distinct bands above the anticipated size of the homodimer that are consistent with higher order multimers; and 2) that creation of stable GB4542-producing cell line pool with removal of all restriction sites resulted in a protein product that contained different ratios of individual moieties than the transient material. (Protein from transiently transfected cell lines was used in all subsequent studies except where indicated.)

Next, we characterized the binding profiles of GB4542 and GB4500 to human B cells and found that both protein products exhibited similar characteristics. Interestingly, GB2542, an sAb with an Fc tail identical to GB4542, but bearing a Fab directed against Her-2, also bound to B cells at higher concentrations. However, G001, a recombinant human IgG1 Fc control, did not bind to human B cells (Fig. 1C). In order to confirm that the observed binding of GB2542 to B cells was mediated by Fc–FcγR interactions, we performed an additional set of studies on Ramos cells, which express CD20 but lack FcγRIIb. As anticipated, even at high concentrations, GB2542 did not bind Ramos (data not shown). The specificity of GB4542 for CD20 was further established in a competition assay with GB4500 (Fig. 1D). These

Table I. Binding kinetics of GB4500 and GB4542 to the canonical FcγRs

| | Apparent $K_D$ ($mol^{-1}$) | | ka ($1/ms \times 10^5$) | | kd ($[1/s]^{-1}$) | |
|---|---|---|---|---|---|---|
| | GB4500 | GB4542 | GB4500 | GB4542 | GB4500 | GB4542 |
| FcγRI | 1.0 ± 0.02E9 | 1.2 ± 1.3E13 | 2.3 ± 0.07 | 26.5 ± 0.2 | 5.5 ± 0.05E4 | 3.2 ± 3.5E7 |
| FcγRIIa | 3.7 ± 0.5E6 | 5.0 ± 0.4E8 | 4.5 ± 0.6 | 2.0 ± 0.1 | 1.7 ± 0.4 | 9.9 ± 0.3E3 |
| FcγRIIb | 4.7 ± 0.6E6 | 4.4 ± 0.02E9 | 1.1 ± 0.2 | 9.2 ± 0.2 | 5.0 ± 1.0E1 | 4.0 ± 0.05E3 |
| FcγRIIIa | 1.6 ± 0.02E7 | 1.0 ± 0.05E10 | 1.6 ± 0.03 | 25.3 ± 0.4 | 2.5 ± 0.06E2 | 2.6 ± 0.09E4 |

His-tagged FcγRs were captured to a CM5 chip using a covalently bound mouse anti-His Ab. For FcγRI and FcγRIIIa, GB4542 and GB4500 were serially diluted from 10 to 0.00064 nmol and 200 to 0.0128 nmol, respectively. For FcγRIIa and FcγRIIb, GB4542 and GB4500 were serially diluted from 5000 to 1.32 nmol. Diluted samples were injected at 25 μl/min for 3 min followed by a 5-min dissociation phase. All curves were run in triplicate. A mouse anti-His–bound surface was used as a reference surface, and blank runs were subtracted from all curves. $K_D$s were calculated using the 1:1 Langmuir model, with refractory index set to zero in the BIAevaluation software version 3.1.

studies revealed that GB4542 competitively inhibited binding of GB4500 to Ramos cells in a concentration-dependent fashion. In contrast, neither IVIG nor GB2542 could inhibit GB4500–CD20 interactions. Collectively, these studies indicate that GB4542 retains its specificity for the rituximab-binding site and that the multimerized Fc domains do not interfere with CD20 engagement.

*GB4542 has improved avidity for the canonical FcγRs*

Next, we determined the ability of GB4542 to bind individual FcγRs using SPR (Supplemental Fig. 2, Table I). In comparison with GB4500, GB4542 bound with greater avidity to FcγRI, FcγRIIa, FcγRIIb, and FcγRIIIa. This increased avidity of GB4542 for the canonical FcγRs was largely due to the extremely low dissociation rates.

*GB4542 preferentially binds B cells versus FcγR-expressing cells in PBMC and colocalizes with FcγR on macrophages*

We next examined the ability of GB4542 to bind FcγR-expressing cells in peripheral blood (Fig. 2). In whole PBMC, both GB4542 and GB4500 demonstrated high levels of B cell recognition, whereas G001 did not bind. At high concentrations, only GB4542 bound $CD20^-$ NK cells, monocytes, and granulocytes. Interestingly, the binding of GB4542 to FcγR-expressing cells was significantly enhanced when B cells were depleted from PBMC. In contrast, GB4500 and G001 had similar background binding to FcγR-expressing cells, regardless of the presence or absence of B cells. Consistent with the role of the multimerized Fc in mediating these interactions, GB2542 demonstrated increased binding to NK cells, monocytes, and granulocytes, in comparison with GB2500, a correlate homodimeric control (Supplemental Fig. 3). These data suggest that, in whole blood, GB4542 preferentially recognizes CD20-expressing cells and, in comparison with GB4500, also has increased capacity to engage FcγR-expressing effector populations. Following B cell depletion, GB4542 has increased capacity to bind $CD20^-FcγR^+$ cells.

In order to visualize potential interactions between GB4542 and FcγR-expressing cells, we investigated the properties of GB4542 colocalization with FcγRII on human macrophages by confocal microscopy. At 0.1 μg/ml, GB4500 was not visible. Following

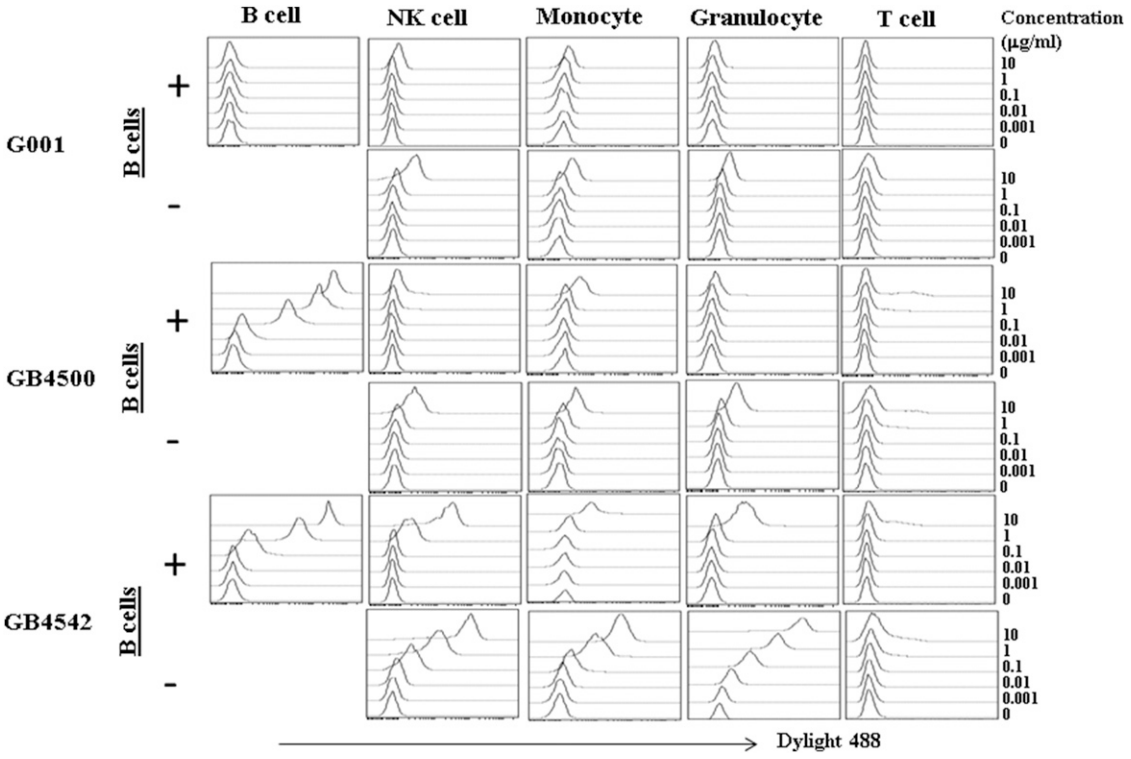


**FIGURE 2.** GB4542 binds $CD20^-FcγR^+$ human PBMC in the presence or absence of B cells. PBMCs with or without B cell depletion were stained with serial dilutions of Dylight 488–labeled G001, GB4500, or GB4542, in combination with immune cell markers. The binding of mAb and sAb with B cells ($CD3^-CD19^+$), NK cells ($CD3^-CD56^+$), monocytes ($CD14^+$), granulocytes ($CD16^+$), and T cells ($CD3^+$) was analyzed by FACS. Results are shown as histogram overlay of serial concentrations of each Ab within different cell population. Data represent one of three experiments using different donors.

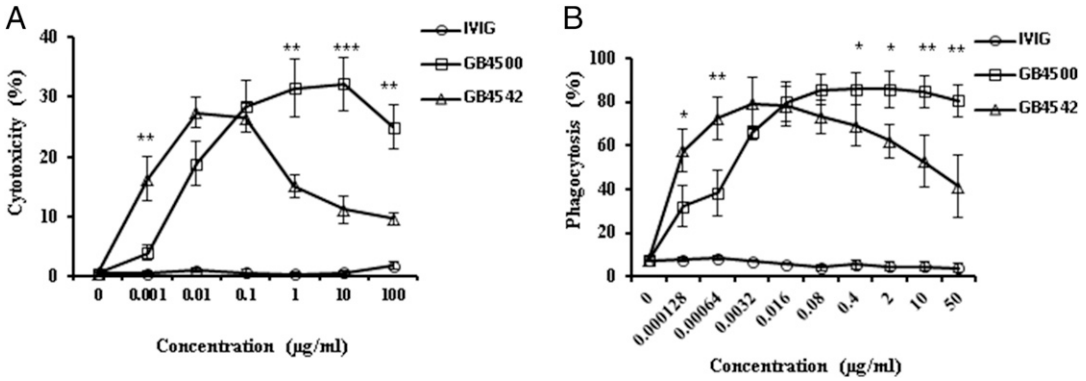


**FIGURE 3.** Low concentrations of anti-CD20 sAb enhance FcγR-mediated B cell depletion, whereas high concentrations have reduced efficacy. The ability of GB4542 and GB4500 to mediate Fc effector functions was determined by ADCC (**A**) and ADCP (**B**) assays. NK cells (A) and macrophages (B) were used as effector cells, and purified normal human B cells were used as targets. The results are shown as the mean ± SEM of four (ADCC) or three (ADCP) experiments with different donors. $*p < 0.05$, $**p < 0.01$, $***p < 0.005$.

incubation of macrophages with GB4500 at a concentration of 10 μg/ml, we observed a diffuse pattern of staining for both CD32 and GB4500. In contrast, at both 0.1 and 10 μg/ml, GB4542 was visible and colocalized with CD32 (white arrows), in a discrete punctate pattern (Supplemental Fig. 4). These data suggest that GB4542 both colocalizes with CD32 and alters its location in/on macrophages.

*Low concentrations of GB4542 mediate potent ADCC and ADCP, which are abrogated at higher concentrations*

Based on the improved binding of GB4542 to FcγR-expressing effector cells, we hypothesized that GB4542 would enhance Fc–FcγR-mediated effector functions. Consistent with this hypothesis, the optimal concentration of GB4542 required for both ADCC and ADCP was about one log order lower than GB4500. However, unlike GB4500, higher concentrations of GB4542 suppressed B cell killing in both assays (Fig. 3A, 3B).

*An Fc analog of GB4542 (GB2542) inhibits mAb-mediated ADCC and ADCP*

In order to determine whether the Fc fragments of GB4542 were inhibiting FcγR- dependent B cell killing, we studied the ability of GB2542 to protect B cells from GB4500- mediated ADCC and ADCP (Fig. 4A, 4B). As anticipated, GB2542 protected B cells from both ADCC and ADCP in a concentration-dependent fashion. Importantly, the concentrations at which these protective effects were observed were consistent with the inflection point at which the ability of GB4542 to mediate these effector functions began to decline. Furthermore, although analogous concentrations IVIG did not inhibit ADCC or ADCP, inhibition of ADCP was

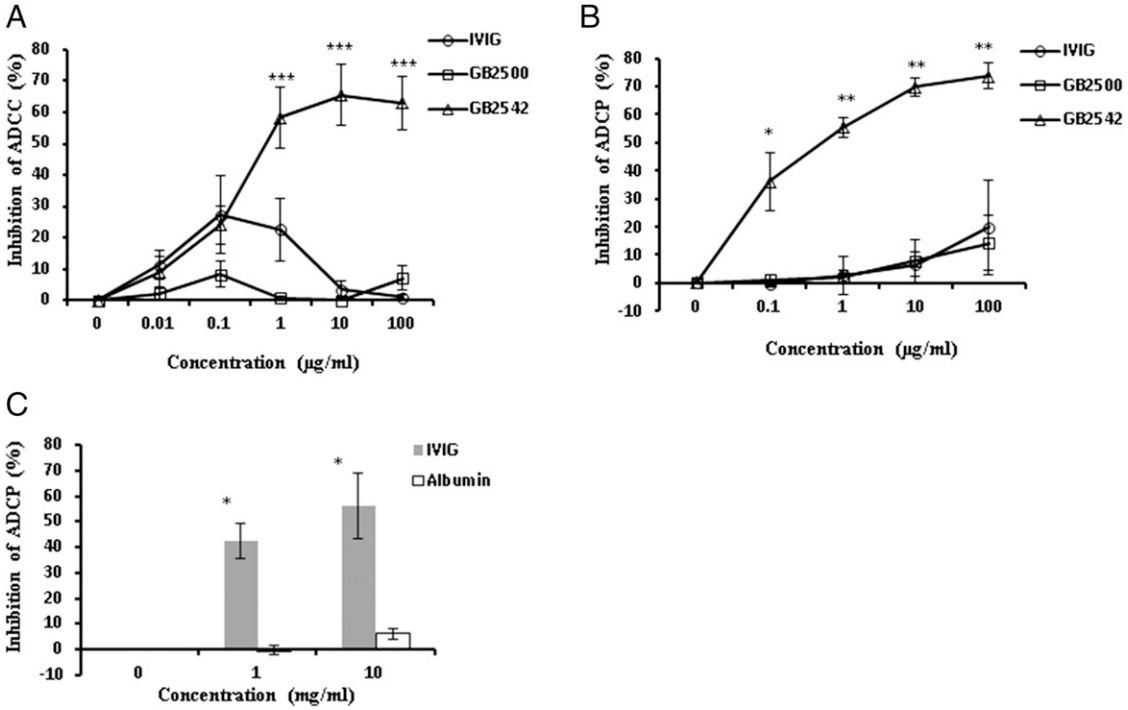


**FIGURE 4.** The inhibition of ADCC and ADCP is dependent on Fc multimerization, and these inhibitory effects can be recapitulated by high-dose IVIG. (**A** and **B**) Inhibition of ADCC and ADCP were evaluated by adding GB2500, GB2542, or IVIG to the cocultures of NK and B cells (ADCC) or macrophage and B cells (ADCP) in the presence of GB4500 at 1 μg/ml (ADCC) or 0.1 μg/ml (ADCP). The results are shown as percent of inhibition relative to controls without treatment. (**C**) High concentrations of IVIG inhibit GB4500-mediated ADCP. Data are mean ± SEM of four (A) or three (B and C) experiments from different donors. $*p < 0.05$, $**p < 0.01$, $***p < 0.005$, GB2542 versus GB2500 (A and B) or IVIG versus albumin (C).

present at 1 mg/ml and was increased at 10 mg/ml (Fig. 4C). These data demonstrate that at concentrations >0.1 μg/ml, the multimerized Fc tails of a GB4542-like sAb can inhibit Ab-mediated B cell death and, in the case of ADCP, mimic the Fc blocking functions of IVIG at ~3-log order lower drug concentrations.

*GB4542 efficiently blocks the binding of human Fc multimers to cells expressing FcγRIIa, -IIb, and -IIIa*

Based on the enhanced binding avidity of GB4542 with FcγRs (Fig. 2, Table I) compared with GB4500, we asked whether GB4542 or its Fc analog directly blocks aggregated Fc–FcγR interactions, thereby inhibiting FcγR-mediated effector functions, such as ADCC and ADCP. In order to address this question, we generated stable CHO cells lines expressing FcγRIIa, FcγRIIb, and FcγRIIIa. GB4542 effectively bound FcγRIIa, FcγRIIb, and FcγRIIIa-expressing cells at concentrations of 0.01, 0.01, and 0.1 μg/ml, respectively (Fig. 5A). Furthermore, in comparison with GB4542, GB4500 only evidenced binding to these cell lines at 2-log order higher concentrations, demonstrating the influence of Fc multimerization on binding to these low-affinity FcγRs.

We next evaluated the ability of GB4542 to inhibit binding of a fully recombinant Fc multimer, GL-2045. As shown in Fig. 5B, GB4542 blocked GL-2045 binding to cells transfected with FcγRIIa, FcγRIIb, and FcγRIIIa in a concentration-dependent fashion. Furthermore, IVIG at concentrations of 1 and 10 mg/ml demonstrated inhibitory effects, whereas no effect was observed with IVIG at concentrations ≤0.1 mg/ml (data not shown). These data demonstrate GB4542 can inhibit Fc multimer binding to FcγRIIa, FcγRIIb, and FcγRIIIa in a manner similar to high concentrations of IVIG.

*GB4542 mediates potent CDC and its Fc analog inhibits mAb-mediated complement activation*

In addition to interacting with FcγRs, aggregated Fcs, but not their homodimeric counterparts, can activate the classic pathway of the complement cascade. Therefore, we next sought to understand whether GB4542 would mediate enhanced CDC. At a concentration of 0.08 μg/ml, GB4542 statistically enhanced CDC in comparison with GB4500. This enhanced killing was durable up to the highest concentration tested (50 μg/ml) (Fig. 6A).

C1q fixation on Ab-coated target cells initiates the classical complement activation cascade and is dependent on the aggregation of Fc. We therefore assessed whether GB4542 mediated enhanced C1q fixation on the B cell surface. Our results indeed showed that, compared with GB4500, GB4542 mediated significantly increased C1q deposition on the surface of B cells corresponding to the observed increase in CDC activity (Fig. 6B).

We subsequently wanted to know whether the multimerized Fc fragments in GB4542 could protect B cells from CDC. GB2542, at a concentration of 0.1 mg/ml, protected B cells from GB4500-mediated CDC (Fig. 6C). Although equivalent doses of IVIG offered only minimal protective effects, a 2-log order higher concentration of IVIG (10 mg/ml), inhibited CDC by ~80%. Interestingly, whereas GB2542-mediated inhibition of CDC was associated with decreased C1q deposition on the B cell surface, protective concentrations of IVIG did not mediate an analogous reduction in C1q deposition (Fig. 6D). Furthermore, in a cell-free ELISA-based C1q binding assay, soluble GB4542 exhibited significantly enhanced C1q binding (Fig. 6E). Collectively, these data indicate that GB4542-like sAb can inhibit mAb-mediated CDC, likely by engaging C1q away from the surface of $CD20^+$ cells.

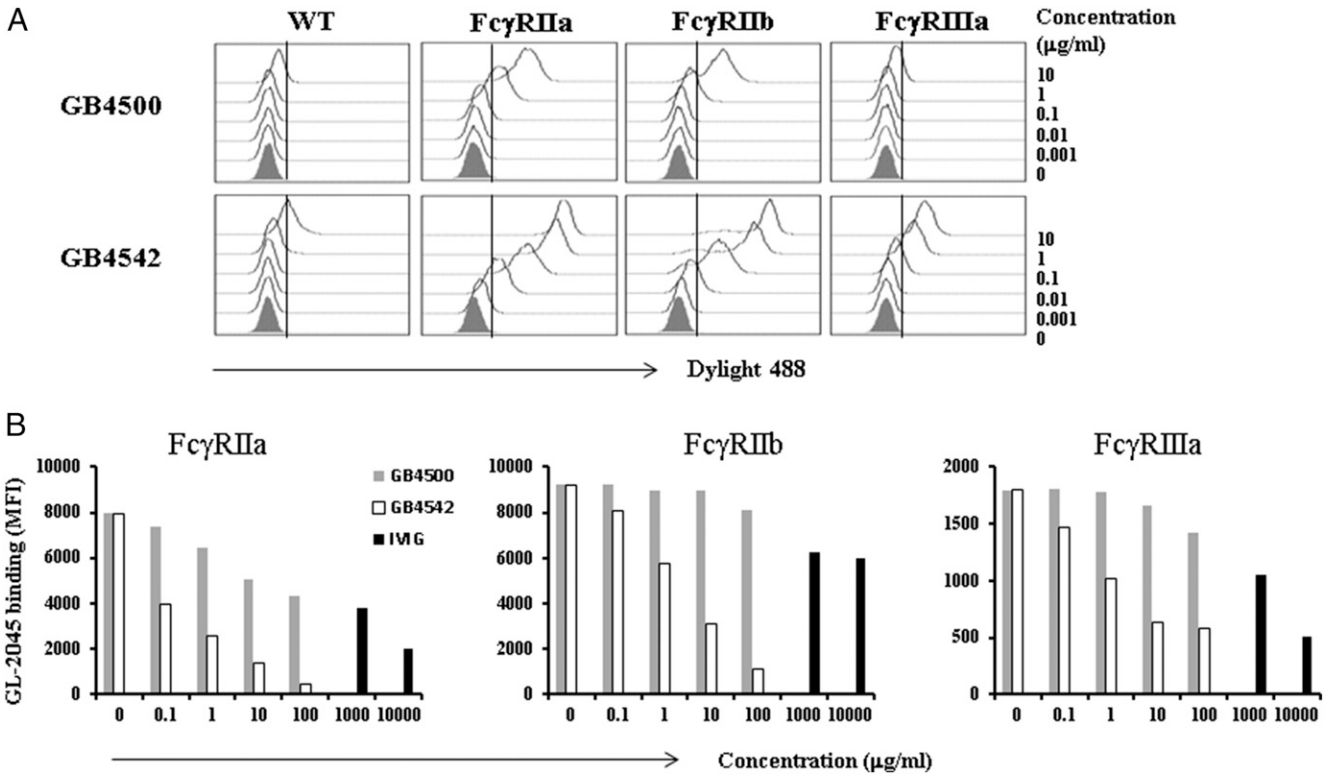


**FIGURE 5.** GB4542 inhibits Fc multimer binding to cell-surface FcγRIIa, FcγRIIb, and FcγRIIIa. (**A**) GB4542 binds FcγR-expressing CHO transfectants. CHO cells expressing human FcγRIIa, -IIb, and -IIIa were stained with serial dilutions of Dylight 488–labeled GB4500 or GB4542 and analyzed by FACS. (**B**) CHO cells expressing human FcγRIIa, -IIb, and -IIIa were pretreated with defined concentrations of GB4500, GB4542, or IVIG for 15 min at room temperature, followed by incubation with Dylight 488–conjugated GL-2045 (human IgG1–based Fc multimer). The binding of GL-2045 with each CHO cell lines was evaluated by FACS analysis. Results are shown as GL-2045 mean fluorescence intensity (MFI) on individual human FcγR-expressing CHO cell lines. Data are representative of three experiments. WT, wild-type.

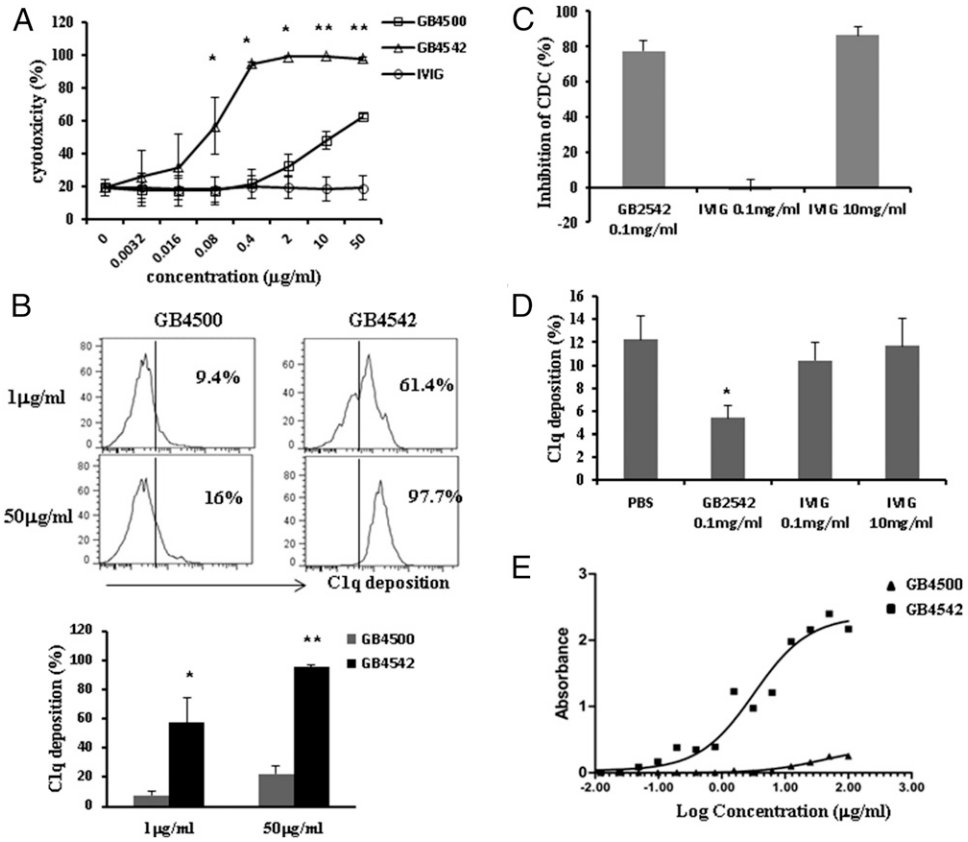


**FIGURE 6.** GB4542 mediates potent CDC, and its Fc analog inhibits mAb-mediated complement activation. (**A**) GB4500, GB4542, and IVIG were evaluated for their ability to mediate CDC against purified human B cell targets using human complement. Data are mean ± SEM of three experiments from different donors. (**B**) B cells were treated with GB4500 or GB4542 at indicated concentration in the presence of human complement for 15 min at 37˚C. C1q deposition was determined by staining cells with anti-C1q Ab and analyzed by flow cytometry. Data are shown as a representative staining and the summarized percent of C1q deposition (mean ± SEM) from three experiments. Inhibition of CDC (**C**) and C1q deposition (**D**) by GB2542 and IVIG. GB2542 and IVIG were preincubated with B cells in the presence of complement at indicated concentration for 15 min at room temperature, and GB4500 (10 μg/ml) was subsequently added to the culture to induce CDC. Data are mean ± SEM of three experiments. (**E**) Soluble GB4542 engages with C1q. The binding of GB4542 and GB4500 with plate-bound C1q was tested in a C1q ELISA assay. Statistical analysis was performed comparing GB4500 versus GB4542 (A and B) or GB4542 versus PBS (D). $*p < 0.05$, $**p < 0.01$.

*The high and low m.w. fractions of GB4542 mediate distinct effector functions*

GB4542 was designed to improve the binding with FcγRs by increasing the Fc valency through multimerization. To understand whether different levels of Fc multimerization altered the binding of GB4542 to individual FcγRs, we studied the lower- and higher-order multimer components of GB4542, fraction 2 and fraction 4 from transient transfection pool, respectively. The dissociation rates of TF4 with all the FcγRs were lower than TF2, which resulted in decreased apparent $K_D$s for TF4 binding to the canonical FcγRs than those for the TF2 (Supplemental Fig. 2, Table II). These data demonstrate that, in keeping with our hypothesis, GB4542 contains individual functional fractions and that the higher-order multimers have enhanced avidity for the FcγRs tested.

Next, we sought to understand how the concentration-dependent effector functions of GB4542 related to the individual multimer fractions within the combined preparation. In the ADCP assays, although both TF2 and TF4 exhibited concentration-dependent bimodal effects, in general, TF2 mediated more potent phagocytic activity in all of the tested donors (Fig. 7A). Interestingly, the different GB4542 fractions mediated profoundly different patterns of CDC (Fig. 7B). Specifically, although TF2 recapitulated the CDC data obtained with the unfractionated material, TF4 was less potent in inducing complement-mediated killing. In addition, and unlike TF2 or GB4500, TF4 inhibited CDC by ~80% at 50 μg/ml.

To confirm that different levels of GB4542 polymerization mediated distinct effector functions, we capitalized on our ability to obtain more distinct fractions from supernatant derived from the stable versus the transient pools. Similar to the transient fractions, the lower m.w. SF (SF1) demonstrated greater ADCP and CDC activity than higher m.w. SF (SF4). Although all of the fractions mediated a dose-dependent bimodal effect in the ADCP assay, only SF3 and SF4 decreased CDC activity at high concentrations, which likely reflects the idea that interactions between Fc–FcγR and Fc–complement require different levels of Fc aggregation (Fig. 7C, 7D). These data indicate that ability of GB4542 to enhance Fc-dependent effector functions is largely secondary to the lower-order multimers, whereas the inhibitory effects are most prominent in the higher-order fractions.

*GB4542 and GB4500 induce B cell depletion in PBMC, which is associated with divergent patterns of proinflammatory cytokine release*

Next, we studied the ability of GB4542 to mediate B cell depletion in human PBMC. At concentrations <0.1 μg/ml, GB4542 mediated more potent B cell depletion than GB4500 (Fig. 8A). In contrast, at concentrations >0.1 μg/ml, whereas GB4500 maintained its capacity for B cell depletion, increasing concentrations

Table II. Binding kinetics of GB4542 fractions to the canonical FcγRs

| | Apparent $K_D$ ($mol^{-1}$) | | ka ($1/ms \times 10^5$) | | kd ($[1/s]^{-1}$) | |
|---|---|---|---|---|---|---|
| | TF2 | TF4 | TF2 | TF4 | TF2 | TF4 |
| FcγRI | 1.6 ± 0.7E11 | 4.8 ± 4.1E14 | 28.6 ± 1.7 | 44.0 ± 0.7 | 4.7 ± 1.9E5 | 2.1 ± 1.8E7 |
| FcγRIIa | 4.0 ± 1.7E6 | 1.2 ± 0.9E7 | 1.0 ± 0.4 | 5.4 ± 0.4 | 3.7 ± 0.6E1 | 6.5 ± 0.08E2 |
| FcγRIIb | 1.6 ± 0.06E7 | 8.9 ± 0.09E9 | 11.5 ± 1.6 | 16.0 ± 0.4 | 1.9 ± 2.3E1 | 1.4 ± 0.3E2 |
| FcγRIIIa | 1.6 ± 0.4E10 | 1.0 ± 0.6E11 | 37.7 ± 5.5 | 43.4 ± 1.4 | 5.9 ± 1.0E4 | 4.3 ± 2.6E5 |

His-tagged FcγRs were captured to a CM5 chip using a covalently bound mouse anti-His Ab. For FcγRI and FcγRIIIa, GB4542 TF2 and TF4 were serially diluted from 1.5 to 0.023 nmol. For FcγRIIa and FcγRIIb, GB4542 TF2 was serially diluted from 750 to 5.9 nmol, and GB4542 TF4 was serially diluted from 150 to 0.29 nmol. Diluted samples were injected at 25 μl/min for 3 min followed by a 5-min dissociation phase. All curves were run in triplicate. A mouse anti-His–bound surface was used as a reference surface, and blank runs were subtracted from all curves. $K_D$s were calculated using the 1:1 Langmuir model, with RI set to zero in the BIAevaluation software version 3.1.

of GB4542 were inversely correlated with B cell loss. Importantly, IVIG, used as a control for homodimeric and aggregated Fc domains, did not mediate an appreciable reduction in B cell numbers.

As a part of these studies, we also sought to understand whether GB4500 and/or GB4542 induced a proinflammatory cytokine response in PBMC. In the presence of LPS, used as a surrogate for systemic inflammation, both GB4500 and GB4542 stimulated IL-12 and TNF-α release (Fig. 8B). The appearance of these cytokines directly correlated with the concentrations of GB4500 and GB4542 required to mediate optimal B cell depletion, with GB4542 stimulating cytokine production at lower concentrations and limited induction of cytokine release at higher concentrations. In contrast, GB4500 continued to stimulate increasing levels of proinflammatory cytokine release at concentrations higher than those required for optimal B cell depletion.

## Discussion

GB4542 was designed to improve engagement of the canonical FcγRs and enhance complement activation by increasing avidity through the creation of Fc multimers as part of drug targeting CD20. This approach differs from other Ab engineering strategies that focus on a single Fc–FcγR interaction. Specifically, strategies such as defucosylation or prolonging off rates to improve CDC are designed to enhance affinity (29, 30). In contrast, the enhanced effector function of GB4542 is premised on an increase in avidity for the low-affinity FcγRs. As such, this strategy mimics naturally occurring polyclonal Ab responses to neo-antigens, in which Fc coverage is enhanced by the availability of Abs against multiple unique epitopes on each antigenic target. The key distinction between GB4542 and polyclonal Ab responses is that the increased avidity of GB4542 enables it to bind low/intermediate-affinity FcγRs and C1q, independent of Ag engagement. In contrast, because polyclonal Abs aggregate at the antigenic site, they cannot

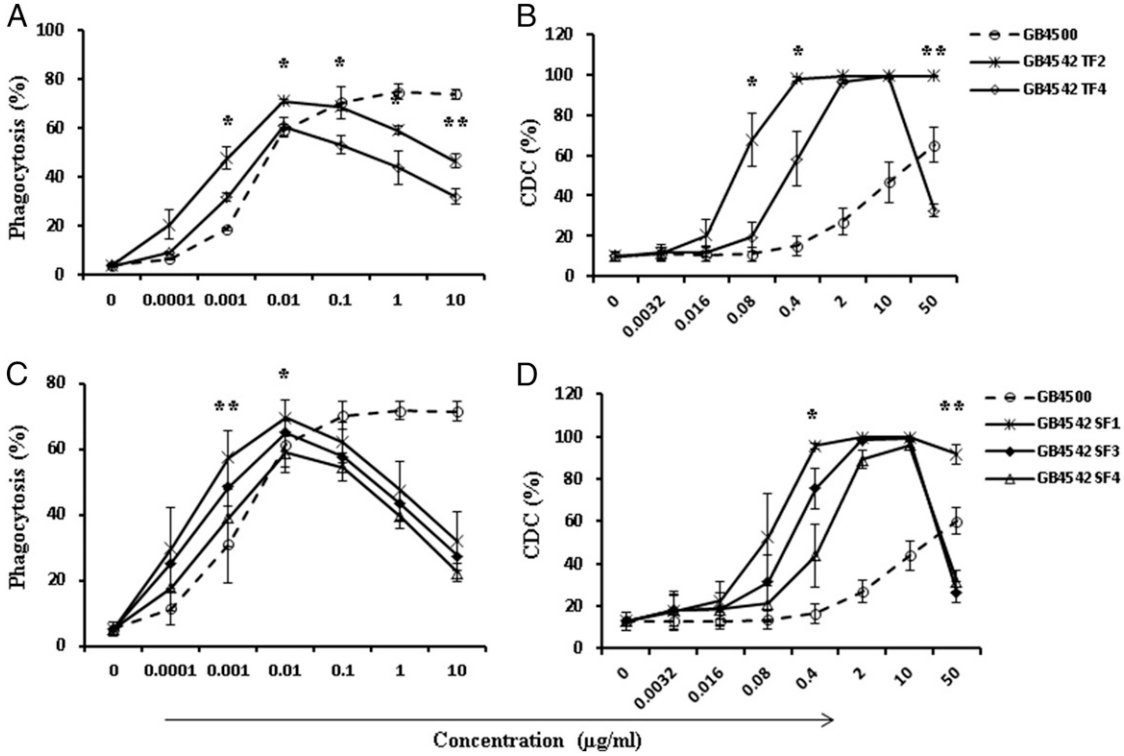


**FIGURE 7.** The high and low m.w. fractions of GB4542 mediate distinct FcγR and complement effector functions. GB4542 fractions from the transient transfection pool (TF) (**A** and **B**) and the stable transfection pool (SF) (**C** and **D**) were evaluated in ADCP (A and C) and CDC (B and D) assays. In the ADCP assays, macrophages were cocultured with CFSE-labeled normal B cells in the presence of serial dilutions of Ab and sAb fractions for 1 h, followed by CD11b staining and FACS analysis. Data are shown as the percentage of macrophage-phagocytosed B cells. In the CDC assay, normal B cells were incubated with serial dilutions of Ab or sAb fractions in the presence of 10% human complement serum for 1 h. Cells were then analyzed for apoptosis/death by flow cytometry. Data are presented as the mean ± SEM of at least three experiments using cells from different donors. $*p < 0.05$, $**p < 0.01$ TF2 versus TF4 (A and B) or SF1 versus SF4 (C and D).

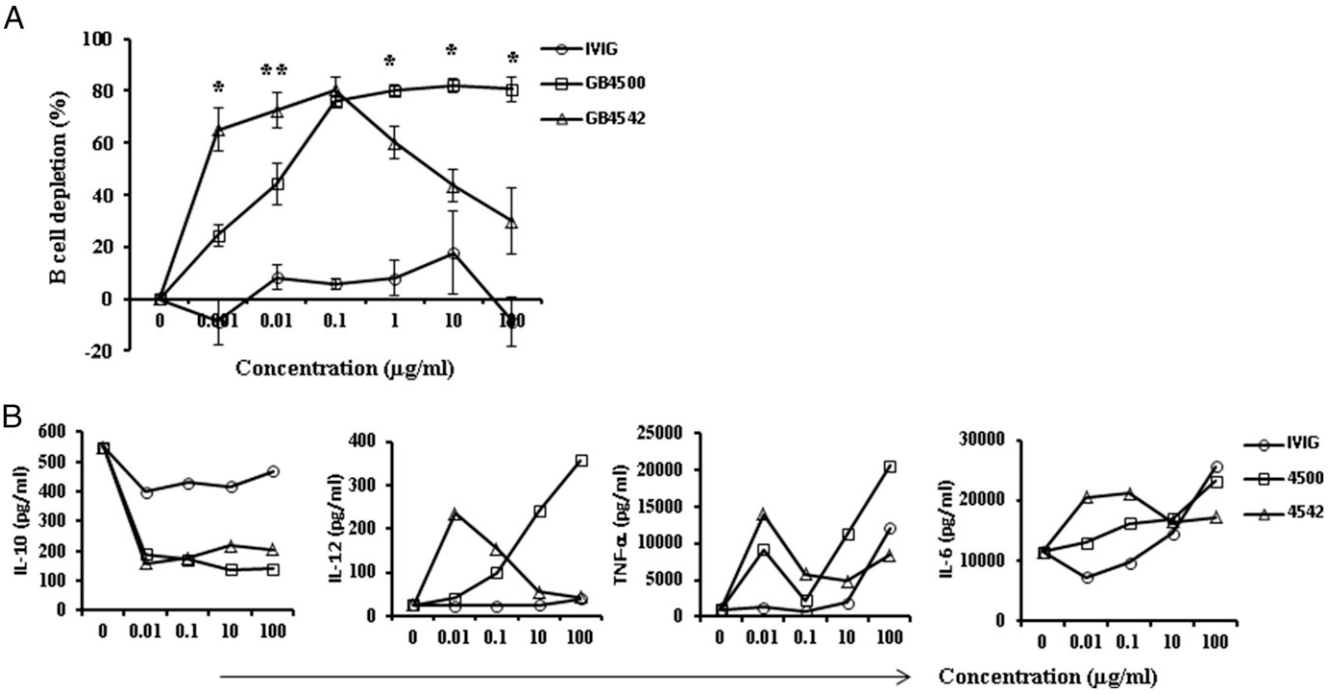


**FIGURE 8.** Low concentrations of GB4542 mediate efficient B cell depletion in PBMC, which is associated with proinflammatory cytokine production. (**A**) PBMCs were cultured in the presence of serial dilutions of GB4500 or GB4542 for 48 h. B cell depletion was determined by FACS analysis of remaining $CD3^-CD19^+$Annexin $V^-$/7-$AAD^-$ cells in the culture relative to untreated controls. The results are the mean and the SEM of four experiments with different donors ($*p < 0.05$, $**p < 0.01$). (**B**) Supernatant was harvested from individual cultures and measured for the cytokines indicated by ELISA. The data shown are one representative of three experiments from different donors.

effectively bind low-affinity FcγRs in the absence of Ag, a fact that limits their ability to induce secondary FcγR-mediated and complement-mediated tolerance (31, 32).

The cDNA construct used to generate GB4542 protein encodes two human IgG1 Fc fragments spaced by IgG2H/ILZ moieties, which is designed to facilitate multimerization (Fig. 1A) (33–36). We previously used this strategy to generate recombinant murine IgG Fc multimers and a recombinant anti-human EGFR sAb (25, 28). SDS-PAGE analysis proved that the resultant protein, GB4542, exists as a homodimer and higher-order multimers. Importantly, the differences in appearance between gels shown in this study and those previously reported by us are consistent with technological variances in the SDS-PAGE systems employed in the two reports, rather than a qualitative changes in GB4542 (28). As anticipated, SPR analysis and FACS-based cellular binding assays revealed that GB4542 demonstrated greatly enhanced avidity to the canonical FcγRs (Fig. 2, Table II). Furthermore, GB4542 showed improved binding to C1q in an ELISA-based assay (Fig. 6E). Importantly, in both cases, this enhanced binding was independent of Ag–Fab interactions.

GB4542 induced potent immunoregulatory effects. Although the mechanisms by which GB4542 mediated enhanced B cell killing at lower concentrations are readily understandable, the means by which it induced FcγR-dependent inhibition at higher concentrations are less clear and are likely pleiotropic. Several recent studies demonstrate that soluble immune complexes (ICs) effectively mitigate defined types of autoimmunity in mice (18) and that high amounts of IC formation during persistent viral infection interfere with Ab effector functions by competition for FcγRs (31, 32). Our studies demonstrated that GB4542 likely mimics the effects of naturally occurring IC by competing for FcγRs and inhibiting Fc–FcγR-dependent effector functions. Importantly, based on data from other groups, it is also possible and indeed plausible that the FcγR-mediated anti-inflammatory properties of GB4542 are not simply passive, but that GB4542 can also actively induce tolerance (16, 38).

In addition to FcγR-mediated functions, mAb-mediated CDC is postulated to be one of the important effector mechanisms in anti-CD20 immunotherapy (29, 38, 39). In vitro studies of CDC activity, using human serum as a source of complement, demonstrated that GB4542 significantly enhanced the B cell killing compared with GB4500. This enhanced killing was associated with increased C1q deposition on the target cell surface. These findings highlight the ability of GB4542 on opsonized B cells to stably engage C1q molecules with profoundly enhanced efficiency compared with GB4500. More importantly, our data demonstrated that GB4542 not only reduced the drug concentration required to induce optimal CDC and C1q deposition, but also increased the maximal level of these activities, at the concentrations evaluated. In keeping with prior reports, the concentrations of GB4542 required to mediate optimal CDC were ~1-log order higher than those needed for B cell depletion from PBMC and phagocytosis (30).

Similar to the inhibitory effects observed for FcγR-dependent functions, GB2542 protected B cells from anti-CD20 mAb-mediated CDC. This protection was associated with reduced C1q deposition that likely resulted from the ability of soluble sAb to effectively engage C1q, independent of Ag–Fab interactions (Fig. 6E). However, unlike GB4542-mediated bimodal effects in ADCC and ADCP assays, GB4542 did not inhibit CDC, even at the highest concentrations tested. These findings are in keeping with data suggesting that different degrees of Fc multimerization are required to elicit FcγR and complement-mediated effects. For example, recent studies revealed the dimeric fraction of IVIG has increased ability of blocking Fc–FcγR interaction over IVIG monomers in macrophage phagocytosis, and a separate report suggested that C1q activation required the formation IgG hexamers (40, 41). Consistent with these findings, whereas both lower- and

higher-order fractions of GB4542 demonstrated decreased ADCP effect at higher concentrations, decreased CDC activity was observed only in the presence of high concentration of higher m.w. fractions (TF4, SF3, and SF4) (Fig. 7).

One of the primary goals of this study was to determine whether GB4542 mediated IVIG-like anti-inflammatory properties. Our data demonstrate that GB4542/2542 and IVIG likely employ both overlapping and distinct mechanisms to mediate their Fc-dependent inhibitory effects. For example, both GB4542 and IVIG blocked Fc–FcγR-mediated ADCC and phagocytosis and inhibited C1q deposition on the cell surface. However, the concentrations of GB4542 required to mediate these inhibitory effects were ~100 times lower than those of IVIG. These data may reflect the fact that IVIG contains only a small portion of multimerized IgGs and are consistent with our animal data in which stradomers could treat or protect animals from autoimmune diseases at a significantly lower dose than IVIG (25). Similarly, although GB2542 blocked Fc multimer binding to all of the low-moderate–affinity human FcγRs tested, IVIG was less effective in blocking FcγRIIb interactions. Furthermore, the inhibitory effect of GB2542 in CDC was associated with blockade of C1q deposition on target cells, whereas IVIG-mediated inhibition of CDC did not impact cell-surface C1q levels under the same experimental settings.

We propose a two-phase model for clinical translation of these findings. In the early phase, or upon initial drug exposure, low concentrations of GB4542 effectively engage CD20 on the B cell surface, where the multimerized Fc domain mediates highly potent B cell depletion. In the late phase, or after reduced CD20 availability secondary to B cell depletion, the multimerized Fc domains of the sAbs can bind C1q and competitively inhibit complement deposition, while also blocking the engagement of immune complexes with FcγR-expressing effector cells. In vivo studies are currently in progress to delineate the most effective dosing strategy and route of administration to achieve long lasting rituximab-like B cell depletion while concomitantly inducing durable IVIG-like tolerogenic effects.

## Disclosures

S.E.S. is a cofounder of and major stockholder in Gliknik Inc., a biotechnology company, and also receives royalties for intellectual property related to B7-H1 (PD-L1), licensed by the Mayo Clinic College of Medicine to third parties. H.S.O, E.Y.M, and D.S.B. are employees of Gliknik. The other authors have no financial conflicts of interest.

## References


1. Cohen, S. B., P. Emery, M. W. Greenwald, M. Dougados, R. A. Furie, M. C. Genovese, E. C. Keystone, J. E. Loveless, G.-R. Burmester, M. W. Cravets, et al; REFLEX Trial Group. 2006. Rituximab for rheumatoid arthritis refractory to anti-tumor necrosis factor therapy: Results of a multicenter, randomized, double-blind, placebo-controlled, phase III trial evaluating primary efficacy and safety at twenty-four weeks. *Arthritis Rheum.* 54: 2793–2806.
2. Edwards, J. C., L. Szczepanski, J. Szechinski, A. Filipowicz-Sosnowska, P. Emery, D. R. Close, R. M. Stevens, and T. Shaw. 2004. Efficacy of B-cell-targeted therapy with rituximab in patients with rheumatoid arthritis. *N. Engl. J. Med.* 350: 2572–2581.
3. Emery, P., F. C. Breedveld, S. Hall, P. Durez, D. J. Chang, D. Robertson, A. Singh, R. D. Pedersen, A. S. Koenig, and B. Freundlich. 2008. Comparison of methotrexate monotherapy with a combination of methotrexate and etanercept in active, early, moderate to severe rheumatoid arthritis (COMET): a randomised, double-blind, parallel treatment trial. *Lancet* 372: 375–382.
4. Emery, P., R. Fleischmann, A. Filipowicz-Sosnowska, J. Schechtman, L. Szczepanski, A. Kavanaugh, A. J. Racewicz, R. F. van Vollenhoven, N. F. Li, S. Agarwal, et al; DANCER Study Group. 2006. The efficacy and safety of rituximab in patients with active rheumatoid arthritis despite methotrexate treatment: results of a phase IIB randomized, double-blind, placebo-controlled, dose-ranging trial. *Arthritis Rheum.* 54: 1390–1400.
5. Mamani-Matsuda, M., A. Cosma, S. Weller, A. Faili, C. Staib, L. Garçon, O. Hermine, O. Beyne-Rauzy, C. Fieschi, J.-O. Pers, et al. 2008. The human spleen is a major reservoir for long-lived vaccinia virus–specific memory B cells. *Blood* 111: 4653–4659.
6. Ramos, E. J., H. S. Pollinger, M. D. Stegall, J. M. Gloor, A. Dogan, and J. P. Grande. 2007. The effect of desensitization protocols on human splenic B-cell populations in vivo. *Am. J. Transplant.* 7: 402–407.
7. Gül, N., L. Babes, K. Siegmund, R. Korthouwer, M. Bögels, R. Braster, G. Vidarsson, T. L. ten Hagen, P. Kubes, and M. van Egmond. 2014. Macrophages eliminate circulating tumor cells after monoclonal antibody therapy. *J. Clin. Invest.* 124: 812–823.
8. Uchida, J., Y. Hamaguchi, J. A. Oliver, J. V. Ravetch, J. C. Poe, K. M. Haas, and T. F. Tedder. 2004. The innate mononuclear phagocyte network depletes B lymphocytes through Fc receptor-dependent mechanisms during anti-CD20 antibody immunotherapy. *J. Exp. Med.* 199: 1659–1669.
9. Taylor, R. P., and M. A. Lindorfer. 2007. Drug insight: the mechanism of action of rituximab in autoimmune disease–the immune complex decoy hypothesis. *Nat. Clin. Pract. Rheumatol.* 3: 86–95.
10. Silverman, G. J., and S. Weisman. 2003. Rituximab therapy and autoimmune disorders: prospects for anti-B cell therapy. *Arthritis Rheum.* 48: 1484–1492.
11. Ahmed, A. R., Z. Spigelman, L. A. Cavacini, and M. R. Posner. 2006. Treatment of pemphigus vulgaris with rituximab and intravenous immune globulin. *N. Engl. J. Med.* 355: 1772–1779.
12. Foster, C. S., P. Y. Chang, and A. R. Ahmed. 2010. Combination of rituximab and intravenous immunoglobulin for recalcitrant ocular cicatricial pemphigoid: a preliminary report. *Ophthalmology* 117: 861–869.
13. Lefaucheur, C., D. Nochy, J. Andrade, J. Verine, C. Gautreau, D. Charron, G. S. Hill, D. Glotz, and C. Suberbielle-Boissel. 2009. Comparison of combination Plasmapheresis/IVIg/anti-CD20 versus high-dose IVIg in the treatment of antibody-mediated rejection. *Am. J. Transplant.* 9: 1099–1107.
14. Vo, A. A., M. Lukovsky, M. Toyoda, J. Wang, N. L. Reinsmoen, C.-H. Lai, A. Peng, R. Villicana, and S. C. Jordan. 2008. Rituximab and intravenous immune globulin for desensitization during renal transplantation. *N. Engl. J. Med.* 359: 242–251.
15. Ikegami, T., A. Taketomi, Y. Soejima, T. Yoshizumi, H. Uchiyama, N. Harada, T. Iguchi, N. Hashimoto, and Y. Maehara. 2009. Rituximab, IVIG, and Plasma Exchange Without Graft Local Infusion Treatment: A New Protocol in ABO Incompatible Living Donor Liver Transplantation. *Transplantation* 88: 303–307 310.1097/TP.1090b1013e3181adcae1096.
16. Siragam, V., D. Brinc, A. R. Crow, S. Song, J. Freedman, and A. H. Lazarus. 2005. Can antibodies with specificity for soluble antigens mimic the therapeutic effects of intravenous IgG in the treatment of autoimmune disease? *J. Clin. Invest.* 115: 155–160.
17. Teeling, J. L., T. Jansen-Hendriks, T. W. Kuijpers, M. de Haas, J. G. J. van de Winkel, C. E. Hack, and W. K. Bleeker. 2001. Therapeutic efficacy of intravenous immunoglobulin preparations depends on the immunoglobulin G dimers: studies in experimental immune thrombocytopenia. *Blood* 98: 1095–1099.
18. Clynes, R. 2005. Immune complexes as therapy for autoimmunity. *J. Clin. Invest.* 115: 25–27.
19. Augener, W., B. Friedmann, and G. Brittinger. 1985. Are aggregates of IgG the effective part of high-dose immunoglobulin therapy in adult idiopathic thrombocytopenic purpura (ITP)? *Blut* 50: 249–252.
20. Deng, R., and J. P. Balthasar. 2007. Comparison of the effects of antibody-coated liposomes, IVIG, and anti-RBC immunotherapy in a murine model of passive chronic immune thrombocytopenia. *Blood* 109: 2470–2476.
21. Bazin, R., R. Lemieux, T. Tremblay, and I. St-Amour. 2004. Tetramolecular immune complexes are more efficient than IVIg to prevent antibody-dependent in vitro and in vivo phagocytosis of blood cells. *Br. J. Haematol.* 127: 90–96.
22. Bazin, R., R. Lemieux, and T. Tremblay. 2006. Reversal of immune thrombocytopenia in mice by cross-linking human immunoglobulin G with a high-affinity monoclonal antibody. *Br. J. Haematol.* 135: 97–100.
23. Pilling, D., N. M. Tucker, and R. H. Gomer. 2006. Aggregated IgG inhibits the differentiation of human fibrocytes. *J. Leukoc. Biol.* 79: 1242–1251.
24. Park-Min, K.-H., N. V. Serbina, W. Yang, X. Ma, G. Krystal, B. G. Neel, S. L. Nutt, X. Hu, and L. B. Ivashkiv. 2007. FcgammaRIII-dependent inhibition of interferon-γ responses mediates suppressive effects of intravenous immune globulin. *Immunity* 26: 67–78.
25. Jain, A., H. S. Olsen, R. Vyzasatya, E. Burch, Y. Sakoda, E. Y. Mérigeon, L. Cai, C. Lu, M. Tan, K. Tamada, et al. 2012. Fully recombinant IgG2a Fc multimers (stradomers) effectively treat collagen-induced arthritis and prevent idiopathic thrombocytopenic purpura in mice. *Arthritis Res. Ther.* 14: R192.
26. Niknami, M., M.-X. Wang, T. Nguyen, and J. D. Pollard. 2013. Beneficial effect of a multimerized immunoglobulin Fc in an animal model of inflammatory neuropathy (experimental autoimmune neuritis). *J. Peripher. Nerv. Syst.* 18: 141–152.
27. Thiruppathi, M., J. R. Sheng, L. Li, B. S. Prabhakar, and M. N. Meriggioli. Recombinant IgG2a Fc (M045) multimers effectively suppress experimental autoimmune myasthenia gravis. *J. Autoimmun.* 52: 64–73.
28. Jain, A., B. Poonia, E. C. So, R. Vyzasatya, E. E. Burch, H. S. Olsen, E. Y. Mérigeon, D. S. Block, X. Zhang, D. H. Schulze, et al. 2013. Tumour antigen targeted monoclonal antibodies incorporating a novel multimerisation domain significantly enhance antibody dependent cellular cytotoxicity against colon cancer. *Eur. J. Cancer* 49: 3344–3352.
29. Bologna, L., E. Gotti, F. Da Roit, T. Intermesoli, A. Rambaldi, M. Introna, and J. Golay. 2013. Ofatumumab is more efficient than rituximab in lysing B chronic lymphocytic leukemia cells in whole blood and in combination with chemotherapy. *J. Immunol.* 190: 231–239.
30. Teeling, J. L., R. R. French, M. S. Cragg, J. van den Brakel, M. Pluyter, H. Huang, C. Chan, P. W. H. I. Parren, C. E. Hack, M. Dechant, et al. 2004. Characterization of new human CD20 monoclonal antibodies with potent cytolytic activity against non-Hodgkin lymphomas. *Blood* 1793–1800.

31. Yamada, D. H., H. Elsaesser, A. Lux, J. M. Timmerman, S. L. Morrison, J. C. de la Torre, F. Nimmerjahn, and D. G. Brooks. 2015. Suppression of Fcγ-receptor-mediated antibody effector function during persistent viral infection. *Immunity* 42: 379–390.
32. Wieland, A., R. Shashidharamurthy, A. O. Kamphorst, J. H. Han, R. D. Aubert, B. P. Choudhury, S. R. Stowell, J. Lee, G. A. Punkosdy, M. J. Shlomchik, et al. 2015. Antibody effector functions mediated by Fcγ-receptors are compromised during persistent viral infection. *Immunity* 42: 367–378.
33. Yoo, E. M., L. A. Wims, L. A. Chan, and S. L. Morrison. 2003. Human IgG2 can form covalent dimers. *J. Immunol.* 170: 3134–3138.
34. Wypych, J., M. Li, A. Guo, Z. Zhang, T. Martinez, M. J. Allen, S. Fodor, D. N. Kelner, G. C. Flynn, Y. D. Liu, et al. 2008. Human IgG2 antibodies display disulfide-mediated structural isoforms. *J. Biol. Chem.* 283: 16194–16205.
35. Dillon, T. M., M. S. Ricci, C. Vezina, G. C. Flynn, Y. D. Liu, D. S. Rehder, M. Plant, B. Henkle, Y. Li, S. Deechongkit, et al. 2008. Structural and functional characterization of disulfide isoforms of the human IgG2 subclass. *J. Biol. Chem.* 283: 16206–16215.
36. Morris, A. E., R. L. Remmele, Jr., R. Klinke, B. M. Macduff, W. C. Fanslow, and R. J. Armitage. 1999. Incorporation of an isoleucine zipper motif enhances the biological activity of soluble CD40L (CD154). *J. Biol. Chem.* 274: 418–423.
37. Siragam, V., A. R. Crow, D. Brinc, S. Song, J. Freedman, and A. H. Lazarus. 2006. Intravenous immunoglobulin ameliorates ITP via activating Fc gamma receptors on dendritic cells. *Nat. Med.* 12: 688–692.
38. Taylor, R. P., and M. A. Lindorfer. 2008. Immunotherapeutic mechanisms of anti-CD20 monoclonal antibodies. *Curr. Opin. Immunol.* 20: 444–449.
39. Pawluczkowycz, A. W., F. J. Beurskens, P. V. Beum, M. A. Lindorfer, J. G. J. van de Winkel, P. W. H. I. Parren, and R. P. Taylor. 2009. Binding of submaximal C1q promotes complement-dependent cytotoxicity (CDC) of B cells opsonized with anti-CD20 mAbs ofatumumab (OFA) or rituximab (RTX): considerably higher levels of CDC are induced by OFA than by RTX. *J. Immunol.* 183: 749–758.
40. Diebolder, C. A., F. J. Beurskens, R. N. de Jong, R. I. Koning, K. Strumane, M. A. Lindorfer, M. Voorhorst, D. Ugurlar, S. Rosati, A. J. R. Heck, et al. 2014. Complement is activated by IgG hexamers assembled at the cell surface. *Science* 343: 1260–1263.
41. Nagelkerke, S. Q., G. Dekkers, I. Kustiawan, F. S. van de Bovenkamp, J. Geissler, R. Plomp, M. Wuhrer, G. Vidarsson, T. Rispens, T. K. van den Berg, and T. W. Kuijpers. 2014. Inhibition of FcγR-mediated phagocytosis by IVIg is independent of IgG-Fc sialylation and FcγRIIb in human macrophages. *Blood* 124: 3709–3718.

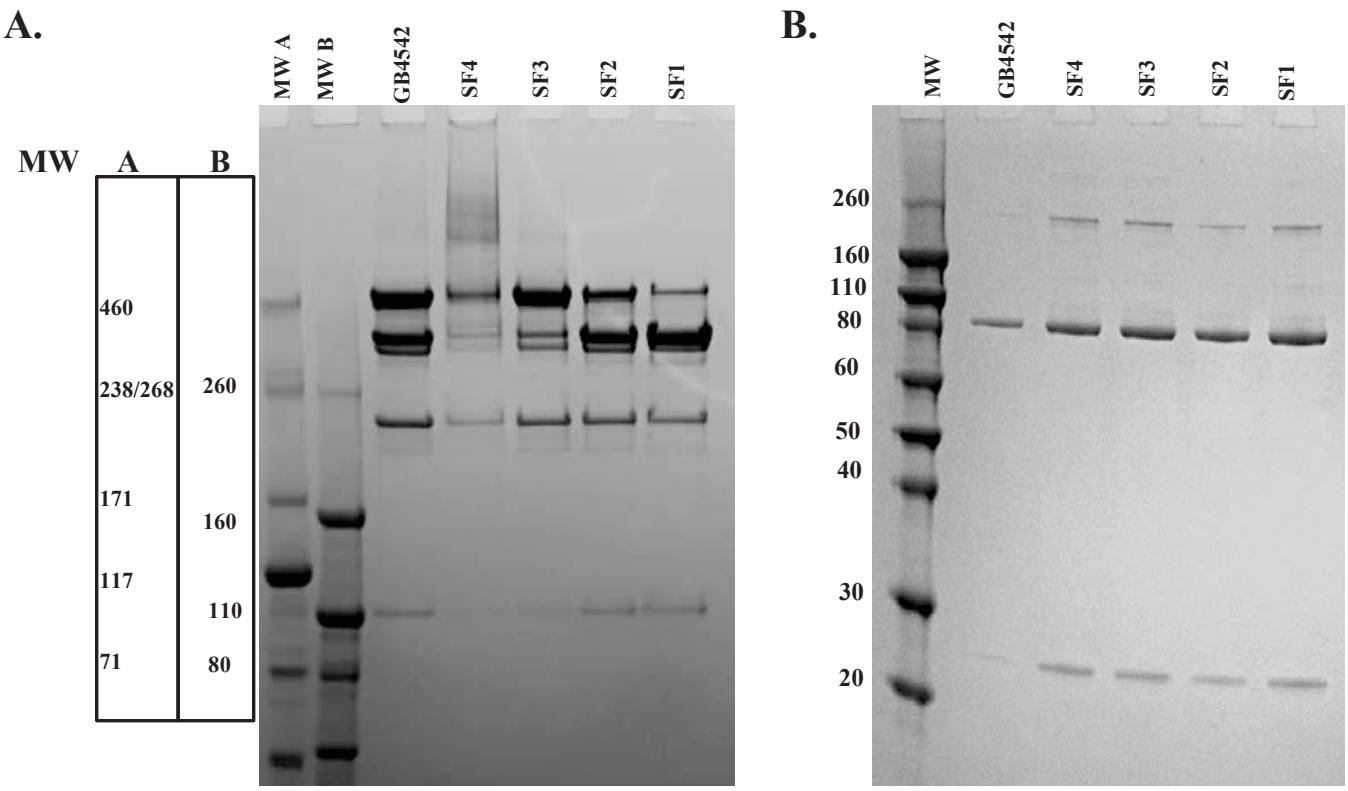


**Supplemental Figure 1. Non-reducing (A) and reducing (B) SDS PAGE analysis of whole and fractionated GB4542 produced by the stable pool.** In order to develop a high fidelity GB4542 protein product, we generated a stable GB4542 producing pool. Exclusion chromatography was employed to better delineate the component of individual fractions and as a means to provide material for functional studies. Non-reducing SDS PAGE analysis of the whole and fractionated proteins (SF 1-4) revealed 4 predominant bands, consistent with the homodimer, and higher order multimers. Under reducing condition, whole and fractions of GB4542 demonstrated identical heavy chain band at around 80 kDa, and light chain band at around 25 kDa.

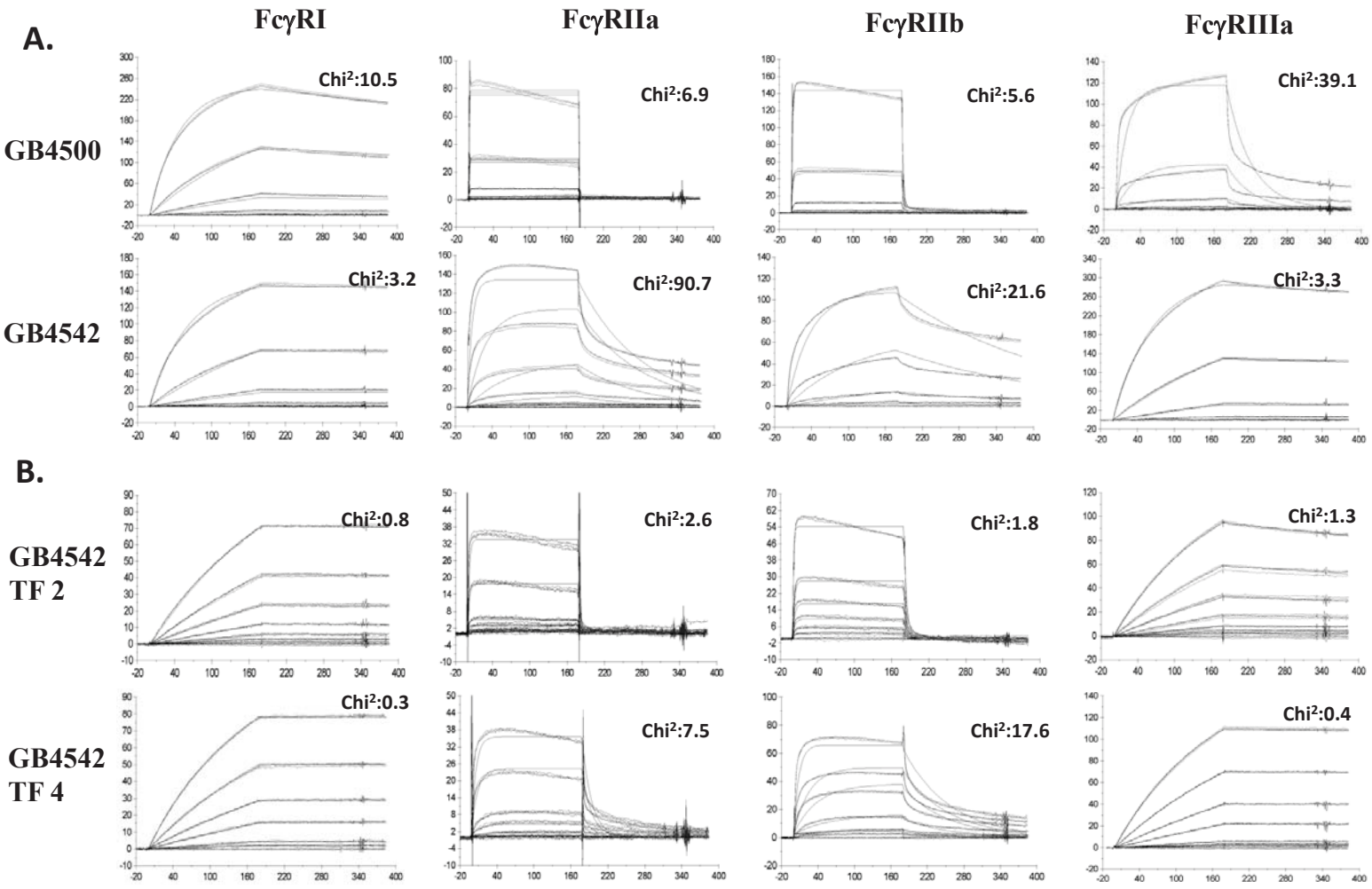


**Supplemental Figure 2. Histograms supporting the numerical data presented in Table 1 and 2.** SPR analysis of the GB4500 vs GB4542 (A), GB4542 TF2 vs TF4 (B) binding to canonical human FcγRs. GB4542 exhibits dramatically slower dissociation rates compared to GB4500. TF4 exhibited slower dissociation rates compared with TF2, particularly with regard to FcγRIIa and FcγRIIb. $Chi^2$ is a measurement of the fit of the curve.

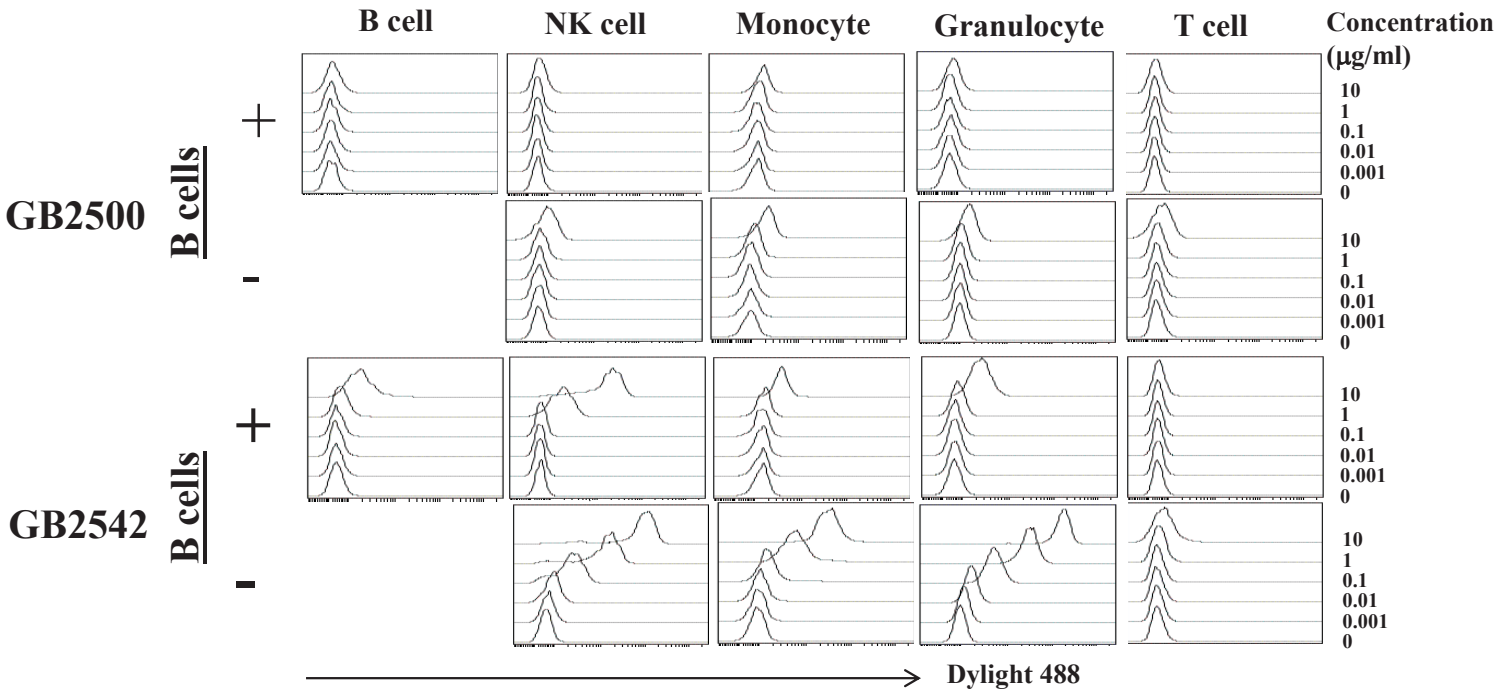


**Supplemental Figure 3: GB2542 binds FcγR expressing immune cells.** PBMCs with or without B cell depletion were stained with serial dilutions of Dylight 488 labeled GB2500 or GB2542, in combination with immune cell markers. Binding was analyzed by FACS.GB2500, an unmodified anti-Her-2 mAb, does not bind peripheral blood cells which lack Her-2 expression. In contrast, multimerized GB2542, binds FcγR expressing PBMC, but does not bind T cells, which lack FcγR expression. These data indicate that the multimerized Fc domains of GB2542, which are identical to GB4542, effectively bind FcγRs on PBMC.

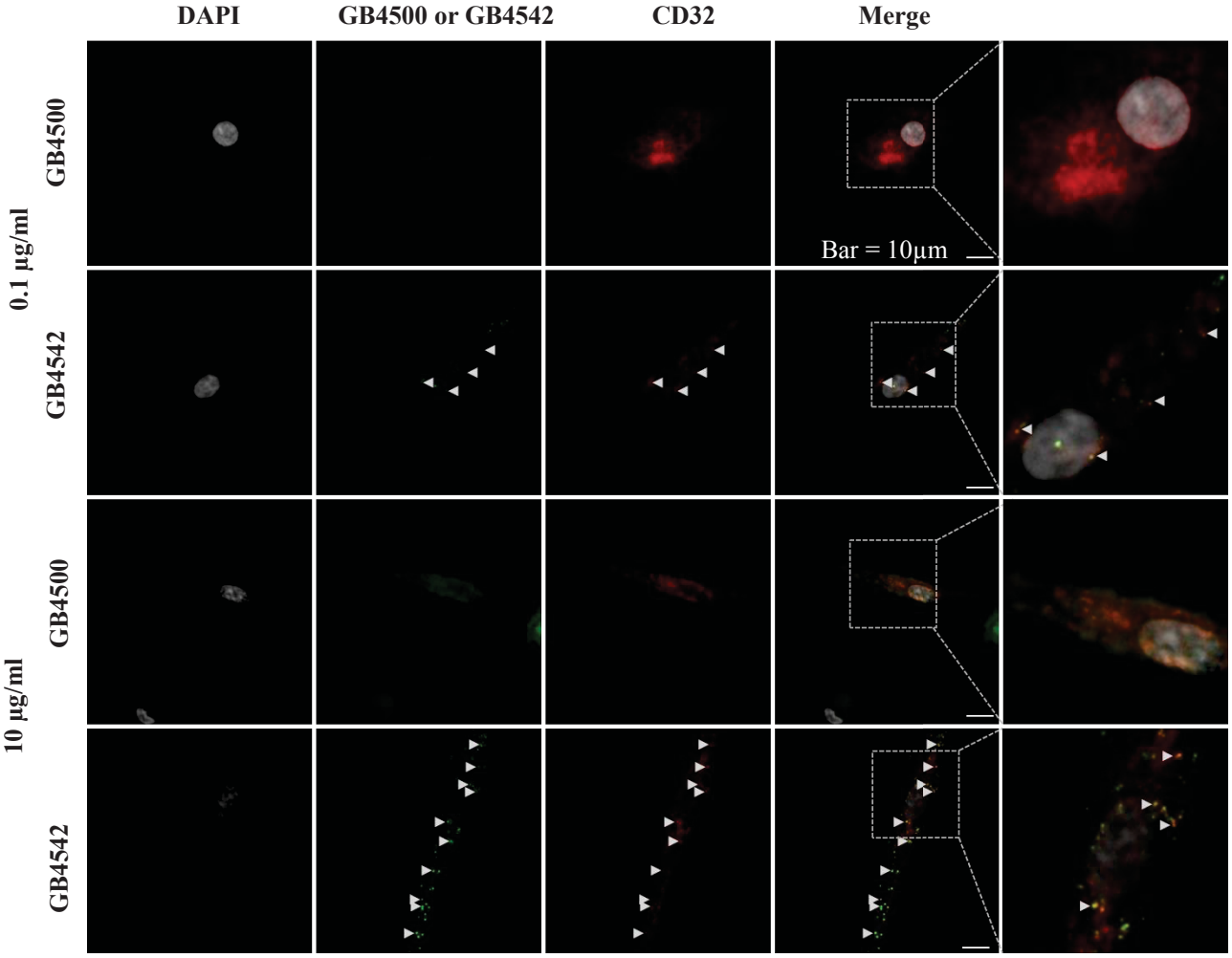


**Supplemental Figure 4. GB4542 co-localized with FcγRII on human macrophages**. In order to understand whether GB4542 interacted with FcγRs on PBMC, we tested its ability to co-localize with FcγRII on human macrophages. At 0.1 µg/ml, GB4500 was not visible. However, following incubation of macrophages with GB4500 at a concentration of 10 µg/ml, we observed a diffuse pattern of staining for both CD32 and GB4500. In contrast, GB4542 was visible by confocal at a concentration of 0.1 µg/ml and co-localized with CD32 (white arrows), in a discrete punctate pattern. These data suggest that GB4542 both co-localizes with CD32 and alters its location in/on macrophages.